The 8th International Supercritical CO_2 Power Cycles Symposium
February 27 – 29, 2024, San Antonio, Texas
Paper #31

The Experimental and Numerical Investigation of Internal Heat Transfer for Supercritical Carbon Dioxide Cooling in a Staggered Pin Fin Array and Single-Jet Impingement

Ryan Wardell*, John Richardson, Marcel Otto, Emmanuel Gabriel-Ohanu, Mathew Smith, Erik Fernandez, Jayanta Kapat
Center for Advanced Turbomachinery and Energy Research
Department of Mechanical and Aerospace Engineering
University of Central Florida
Orlando, FL 32816

Ryan Wardell is a Ph.D. student at the University of Central Florida. His research focuses on sCO2 heat transfer and power cycles. Ryan Wardell is generally interested in sCO2 power cycles and sustainable power generation solutions. He has an Aerospace Engineering B.S. from the University of Central Florida and is working towards his M.S. and Ph.D. in Aerospace Engineering with expected graduation in 2025.

ABSTRACT

Over the past decade, the drive to reduce greenhouse gas emissions and to increase thermal efficiency for turbomachinery has invigorated the application of supercritical carbon dioxide (sCO_2) power cycles for energy generation. Compared to the industry standard air cycles, sCO_2 applications hold the potential for several advantages, including higher efficiencies, smaller footprints, and zero greenhouse gas emissions. However, like any turbomachinery application, the turbine inlet temperature must increase to increase thermal efficiency. This introduces the need for internal cooling features to avoid material failure as operating conditions rise. Two standard features include pin fin turbulators in the trailing edge and jet impingement in the airfoil's leading edge. Over the past several decades, these features have been the subject of extensive research. However, the move to the sCO_2 operating environment creates the need to re-visit these features to quantify the heat transfer capabilities within this supercritical cooling environment. The first objective of this paper is to discuss the development of the experimental demonstration for internal heat transfer testing at 200 bar and 400 Celsius, which sits well within the CO_2 supercritical region. Next, the heat transfer for pin fin turbulators and single-jet impingement in the sCO_2 environment is compared to existing air data-derived correlations to quantify any deviations from literature correlations. Finally, the experimental process aims to validate internal cooling conjugate heat transfer numerical simulations for sCO_2 turbines.

INTRODUCTION

Reducing greenhouse gas emissions has been a leading factor in power cycle development to address the concern of climate change. Although research in renewable resources has presented promising progress, power cycles will continue to provide a large majority of civilization's energy needs. This means that reducing the greenhouse emissions of these power cycles through novel and innovative initiatives is a must. One promising power cycle concept is the supercritical carbon dioxide power cycle (sCO_2), which has arisen from the efforts to develop new power cycles. This cycle utilizes one of the greenhouse gas emissions, CO_2. Utilizing this gas as the operating fluid within these power cycles can reduce emissions, if not eliminate them. The sCO_2 power cycle also provides several advantages by capitalizing on the supercritical nature of CO_2. This has contributed to the growing international popularity of research in the sCO_2 power cycles over the past decade [1]. One of the advantages is the potential for higher thermal efficiencies, which contributes to the considerable appeal of the sCO_2 power cycles. Other advantages include a higher power density, decreasing the footprint of the power cycles for comparable power output, and achieving near-zero greenhouse gas emissions by operating in a closed-loop environment [2]. Another appealing factor of the sCO_2 power cycle is the easily achievable critical point of CO_2. With a more achievable critical point than water, such as in the steam Rankine cycle, the CO_2 power cycle can take advantage of compressing near the critical point while staying single-phased. Compressing near the critical point reduces the necessary work that must be done on the fluid during compression [1]. Exploring these advantages has led to several initiatives to research power cycle concept development and heat exchangers, but this has been the primary focus of literature in the sCO_2 regime.

This has led to several demonstrations of sCO_2 gas turbine technology, the first being NET Power [3]. They developed a direct-fired semi-closed loop, the first demonstration of the advantages of the sCO_2 power cycle working towards achieving near-zero emissions. Southwest Research Institute is developing another demonstration. Their demonstration was named the Supercritical Transformational Electric Power (STEP) demo pilot [4]. This indirect-fired power cycle was designed to be a 10MWe sCO_2 power cycle. One method of increasing the efficiency of these power cycles and increasing the power output of the power cycles is increasing the turbine inlet temperature (TIT). Following the STEP demonstration, Southwest Research Institute has begun developing a 300 MWe direct-fired power cycle to demonstrate the capabilities of sCO_2 power cycles further [5]. Increasing the TIT of the power cycle is one method of increasing the thermal efficiency of the system. However, by continuing to increase the turbine inlet temperature, the turbine geometry must be actively cooled to ensure the material limits of the geometry do not exceed a critical temperature where the material would fail. Internal cooling can be employed in the geometry of the turbine to mitigate this risk and allow higher turbine inlet temperatures. Flow paths are designed within the turbine geometry, introducing a cooling flow within the blades and vanes and active cooling of the turbine components.

Various designs can be involved in internal cooling geometry, including jet impingement throughout the flow path, ribbed serpentine channels that induce turbulence, and pin fin arrays in the trailing edge, to name a few. Internal cooling is not a novel solution to increasing turbine inlet temperatures, with several studies performed over the past decades. However, these geometries were all explored in an air environment, as this is the industry standard for gas turbine technology. Introducing the sCO_2 environment means exploring these geometries again, as the same results and correlations derived using air data can only be said to represent sCO_2 after investigating the heat transfer within the new operating environment. Two different geometries have been explored at the University of Central Florida in the closed sCO_2 loop facility. These two geometric solutions investigated were jet impingement and pin fin arrays. Jet impingement

is commonly used in the leading-edge channels where the blade or vane experiences the highest temperatures. Here, flow is directed through small orifices before impinging onto a surface. In the trailing edge, pin fin arrays increase turbulence in the fluid flow through this region while also providing structural support in this thin region.

As mentioned, several decades of research have been performed for both geometries; however, all this research was done with air as the operating environment. Despite this, reviewing critical research for both geometries is necessary to understand how heat transfer has been studied in the past and how it differs for the sCO_2 environment. Jet impingement will be investigated first, and several researchers have made significant contributions to researching this geometry. Martin, Huang, Sagot, and Goldstein [6_9] explored the heat transfer for single jet impingement by varying the flow rates, jet distance to the impinging surface, and the impinging surface size. These parameters were defined by the diameter of the jet orifice, resulting in a z/D and R/D for each case. The Reynolds numbers, z/D, and R/D, are tabulated in Table 1, along with their resultant Nusselt number correlations for these four studies. These efforts focused on changing the z/D distance to see how jet impingement heat transfer varied.

Author	Reynolds Number ($x10^3$)	z/D	R/D	Nusselt Correlation
Martin [6]	2 - 400	2 - 12	2.5 - 7.5	$Pr^{0.42}\frac{D}{r}\frac{1-1.1\frac{D}{r}}{1+0.1(\frac{H}{D}-6)\frac{D}{r}}ARe^{n}$
Huang [7]	6 - 124	1 - 10	0 – 10	$Pr^{0.42}Re^{0.76}(a+bH+cH^2)$
Sagot [8]	10 - 30	2 - 6	3 – 10	$0.0623Re^{0.8}\left[1-0.168\frac{R}{D}+0.008\left(\frac{R}{D}\right)^2\right]\left(\frac{H}{D}\right)^{-0.037}$
Goldstein [9]	61 - 124	6 - 12	N/A	$\frac{24-\left\lvert\frac{H}{D}-7.75\right\rvert}{533+44\left(\frac{R}{D}\right)^{1.394}}Re^{0.76}$

Table 1: Correlations from literature for single jet impingement

Several studies have been performed on pin fin arrays as well. In the pin fin array, changing orientation, geometry, and other factors have been a primary focus for past literary works. Several studies changing pin fin orientation in staggered pin fin arrays are tabulated in Table 2. The pin fin diameter for a cylindrical pin defined the pin fin array in these studies. This diameter was used to define the spanwise (X/D) and streamwise (Z/D) spacing of the pins, as well as the height of the pins (H/D). This method was adopted from other literary works to provide

a baseline comparison between air and sCO_2. Some notable works included Chyu [10], where inline and staggered configurations were compared for heat transfer enhancement. Ames et al. [11] investigated the effects of turbulence generated in the pin fin array using a staggered cylindrical pin fin array. Metzger and Haley [12] also explored the effects of turbulence and heat transfer by varying the spanwise spacing and changing the pins' conductance. Finally, Otto et al. investigated the cylindrical pin fin array, focusing on the vortical structure formation and endwall heat transfer [13]. These efforts all utilized a cylindrical pin fin shape. Other shapes and geometric definitions were used, but these were the most comparable for the desired efforts of sCO_2 pin fin heat transfer.

Author	Reynolds Number ($x10^3$)	Array Parameters	Nusselt Correlation
Ames [11]	3 – 30	X/D = 2.5 Z/D = 2.5 H/D = 2	$0.0795Re^{0.717}$
Metzger [12]	1.5 - 100	X/D = 2.5 Z/D = 2.5 H/D = 1	$0.069Re^{0.728}$
Chyu [10]	1 – 100	X/D = 2.5 Z/D = 2.5 H/D = 1	$0.08Re^{0.728}Pr^{0.4}$
VanFossen [14]	1 - 60	X/D = 4 Z/D = $2\sqrt{3}$ H/D = 2	$0.153Re^{0.685}$

Table 2: Staggered pin fin correlations from literature

This paper will review the experimental process and numerical validation efforts employed to study single jet impingement and a pin fin array at the University of Central Florida. Richardson et al. [15] and Wardell et al. [16] investigated these investigations independently. The key findings of the results will be explored and explained with a unique insight in this paper; however, further details can be found in Richardson et al.'s and Wardell et al.'s experimental investigations, as well as the numerical investigation for the staggered pin fin array done by Wardell et al. before experimental work began. [17]

METHODOLOGY

At the University of Central Florida's Center for Advanced Turbomachinery and Energy Research, a sCO_2 closed loop has been designed to operate at high temperature and pressure conditions to investigate carbon dioxide within the supercritical regime. This loop was designed to achieve upwards pressures of 260 bar and 550 Celsius for stainless steel piping. This was sufficient to achieve the desired operating conditions for both single jet impingement and staggered pin fin array, which were 200 bar and 400 Celsius. The loop can achieve a maximum flow rate of 0.25 kg/sec, largely dependent on the operating conditions and test section geometry due to the varying thermophysical properties of sCO_2. The complete loop schematic can be seen in Figure 1. The loop consists of a cold and hot side joined through a recuperator, an essential component of the sCO_2 loop design. This is due to the larger specific heat of CO_2, especially

near the pseudo-critical point where the specific heat of CO_2 spikes. Without recuperation, where a large portion of the heat input can be conserved through the system, the loop efficiency would plummet. The recuperator is a large shell and tube configuration.

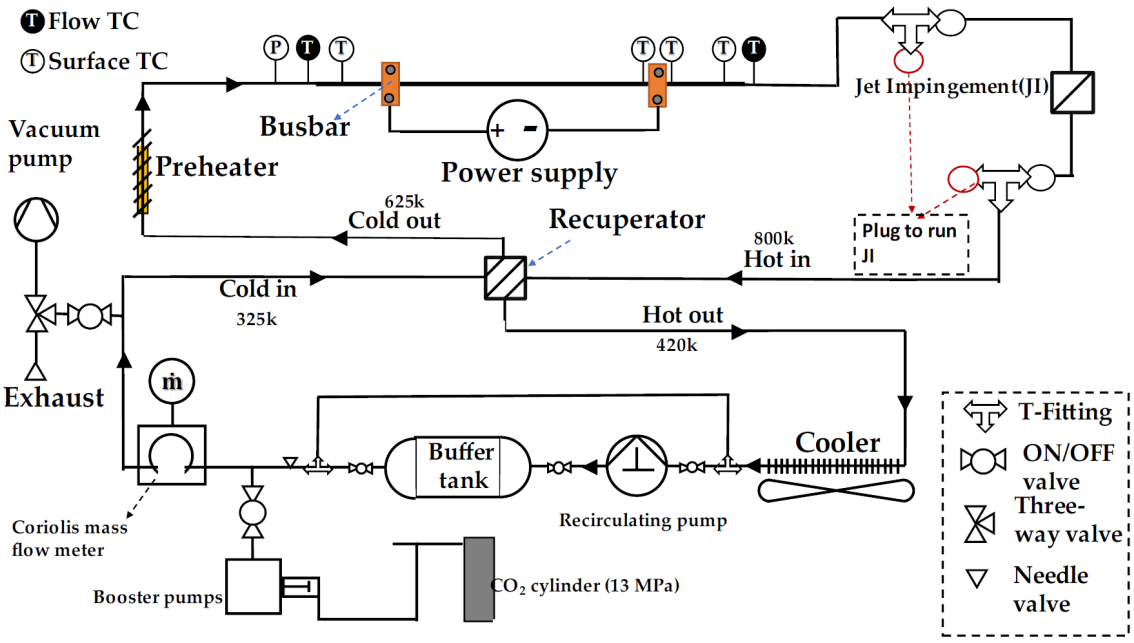

Figure 1: The high temperature and pressure sCO_2 closed loop at the University of Central Florida

The cold side of the loop is where most of the flow controls are located. The loop is vacuumed and filled in this half of the loop where the sigma pump drives the flow. The flow enters a large buffer tank following the sigma pump, where the volume suddenly increases, reducing the oscillations caused by the pump. From there, the flow enters a Coriolis flow meter, measured in kg/min before entering the recuperator as the cold inflow for the recuperator. From there, the flow outflow enters the hot path of the loop where all the heat input into the system occurs. The flow is preheated using two methods of electrical heating. The first is a series of rope heaters rated at 1kW of power and a large rope heater bank where 28 1.2kW rope heaters are designed to push the flow to the desired inlet temperature. The second electrical heating method is Joule heating, where an electric current is flown through the stainless-steel pipe, generating heat. This method is used to maintain and increase the temperature of the loop as it moves from the preheating to the heater bank. From here, the loop is at its hottest point, where the test rig is plumbed into the loop. After leaving the impingement or pin fin rig, the flow is directed back into the recuperator as the hot inflow for the recuperator. The flow is then cooled down to pump operating temperatures of around 40 Celsius after leaving the recuperator by flowing through a serpentine pass convection fan configuration and a large chilled water drum.

The operating conditions are monitored throughout the loop using several thermocouples, probes, and pressure transducers. This allows the recuperator temperature and pressures to be monitored, as well as the hot path of the loop, to ensure operating conditions do not exceed material limits at the given pressure. All instrumentation was monitored and recorded

using a Fluke 2686A-PAI Data Acquisition System (DAQ). The primary locations monitored were the hottest part of the loop/ inlet of the test section rig, the four locations of the shell and tube recuperator, and the pump inlet temperature to ensure optimal operating conditions for the pump. Both rig designs need to be understood and overviewed in the flowing sections, as the details can be found in previously cited studies.

Single Jet Array Impingement:

Single jet impingement was the first array tested in this effort to re-investigate heat transfer within the sCO_2 operating environment. The impingement plate was a copper cylinder of 1.5 inches in diameter and 1 inch in height. This block was instrumented with three thermocouples to quantify the temperature distribution of the block accurately. A circular mica heater in contact with the bottom of the copper cylinder generated this distribution. The top part was the impinging surface, which experienced active cooling. This assembly was housed in a silicate holder wrapped in insulation to help direct the heat flux into the copper cylinder and not to the rest of the assembly. The test rig was designed in three parts. The bottom flange was instrumented with three Conax gland fittings, two of which passed through copper electrodes to power the mica heater and one that passed in the thermocouples for the experiment. This copper cylinder assembly was instrumented and secured onto the bottom flange, with several spacers that allowed for the z/D to be controlled. The top flange consisted of the gas flow inlet that entered a plenum before passing through the 3 mm jet orifice, where the flow then impinges on the lower flange assembly. The flow is then directed out of the rig through the third section of the rig, the large cubic container that houses both flange assemblies, and then directs the flow up and out of the rig and back into the loop. This assembly breakdown can be seen in Figure 2.

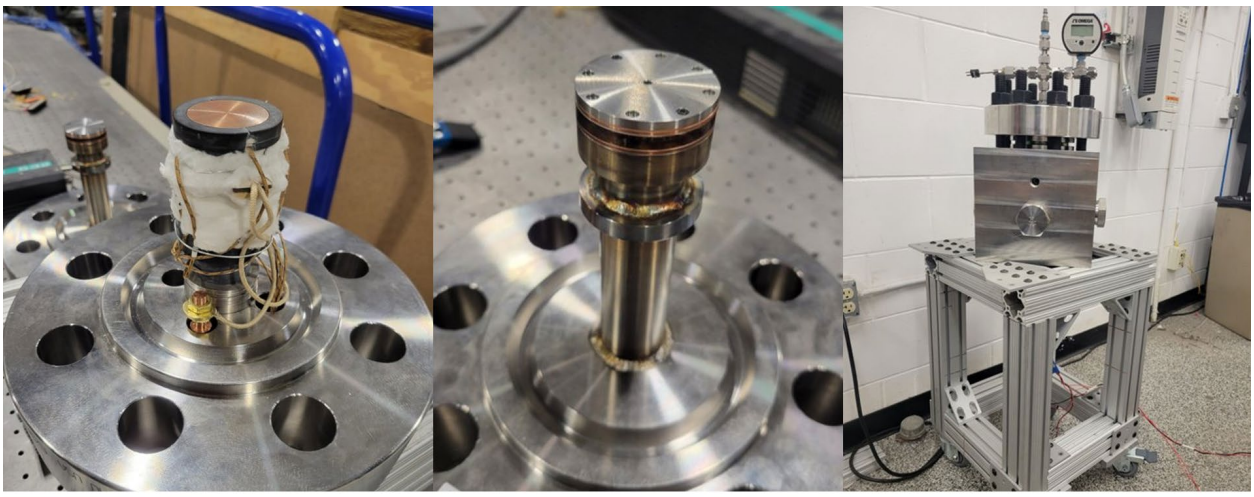

A: Bottom Flange Assembly B: Top Flange Assembly C: Cubic Container Assembly

Figure 2: Bottom flange assembly (A), top flange assembly (B), and full rig assembly (C) for single jet impingement heat transfer for the sCO_2 environment.

At the inlet of the impingement assembly, temperature was measured using a TC probe positioned into the inlet plenum; the jet temperature was calculated by measuring the heat loss through the plenum and backing out the jet temperature. The surface temperature was

calculated through linear approximation by measuring the temperature through the copper block at three locations. These three thermocouples created a linear approximation of temperature across the cylindrical height, starting at the mica heater and going to the surface temperature. This could be done due to copper's high conductivity, as seen in Figure 3.

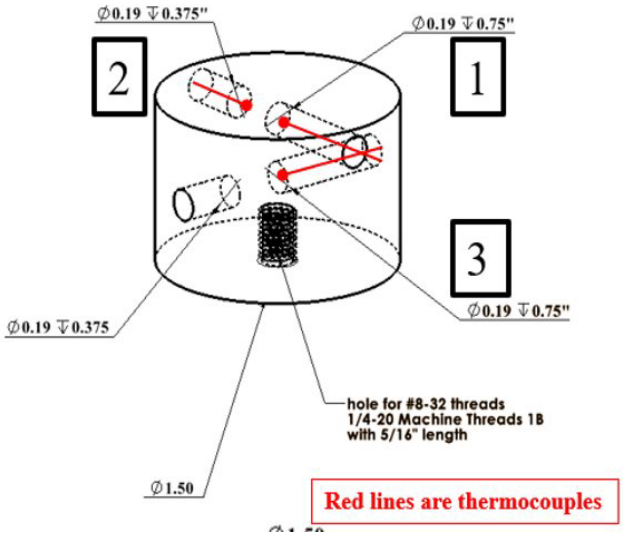

Figure 3: Thermocouple placement within the copper block for single jet impingement

Pin Fin Array

The pin fin array followed the impingement test rig but was tested at the same testing conditions. This rig comprised a large weld neck flange enclosed by two blind flanges. The blind flanges housed the instrumentation and test section plumbing. This assembly was a pressure vessel to encase the test section rig. This prevented the need to engineer the actual pin fin test section to withstand 200 bar pressure. By creating an ambient pressure equal to the flow path pressure within the pressure vessel at any given point, the test section could experience a near-zero pressure differential across the interior and ambient environments. The inlet flange was where the test section plumbing and the Conax glands needed for the thermocouple were secured. The other side of the pressure vessel was the flange instrumented with four Conax glands that passed copper electrodes into the high-pressure environment. This can be seen in Figure 4.

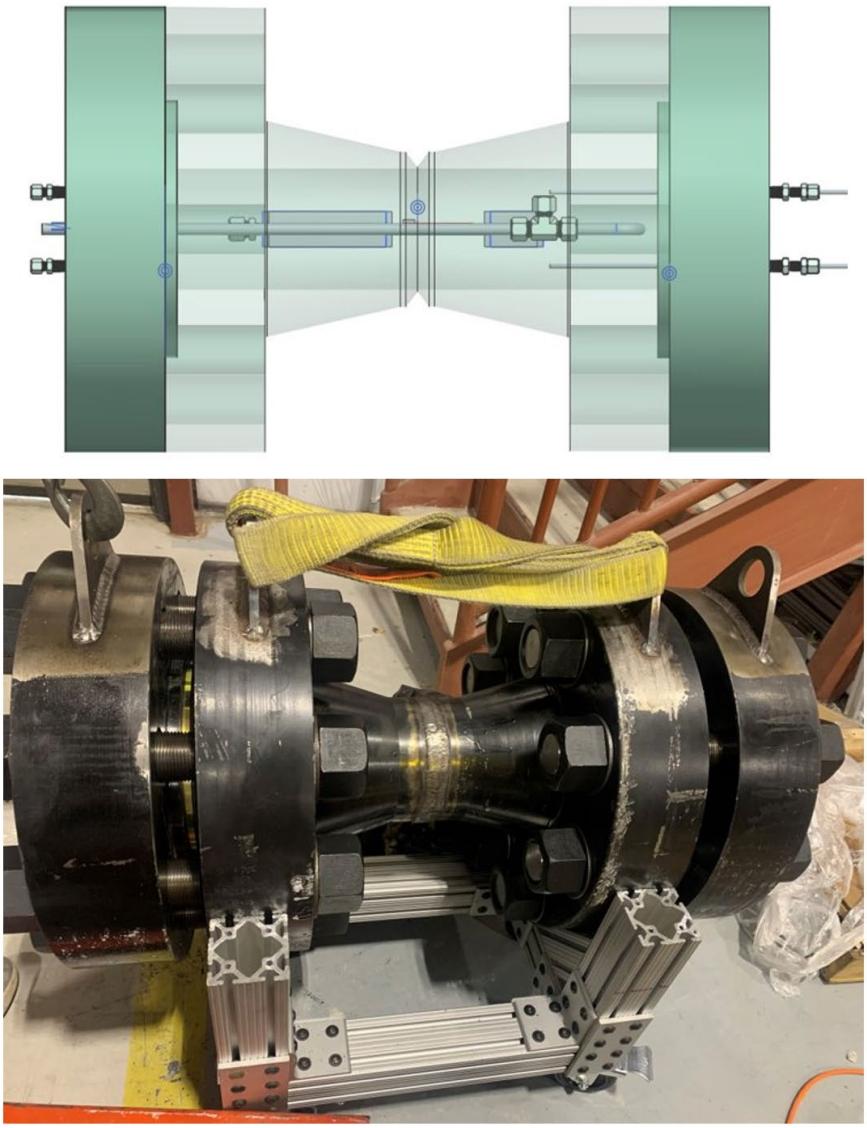

Figure 4: The pin fin pressure vessel for the sCO_2 test rig

These were used to power two rectangular mica heaters on the test section. The test section included the inlet and outlet plumbing attached to the front blind flange. The piping entered a large plenum that stabilized the flow before entering the test section of the pin fin array. This array was designed to match characteristics from literature for direct comparison, which gave an array definition of an x/D and z/D of 2.5 and a h/D of 2. The diameter used for these dimensions was the pin diameter, which was 2mm. After the pin fin array, the flow enters another plenum box before re-entering the loop piping. Immediately after this point, a filter allows the loop gas path to fill and pressurize the chamber to ensure the chamber and internal gas flow path are at near-equal pressures. The test section assembly with the pin fin array is shown in Figure 5.

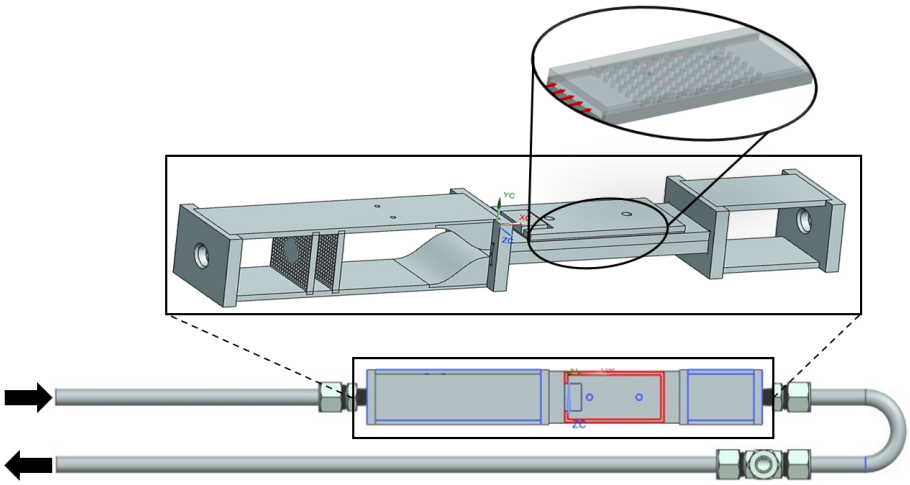

Figure 5: The pin fin test section within the pressure vessel

The test section was instrumented with seven thermocouples. This rig introduced several challenges unique to the pin fin array. In the pin fin configuration, instrumentation was limited. Typical approaches to calculating heat transfer across the pin fin array were to take a local approach, measuring each row and calculating an array average. However, this pin fin experiment utilized a bulk average approach using enthalpy balance to calculate the heat flux of the system. The seven thermocouples were located throughout the test section. Two were upstream of the pin fin test section, two downstream, and one on the top and one on the bottom end walls. The seventh thermocouple was in the ambient pressure vessel to monitor this cavity. These locations can be seen in Figure 6.

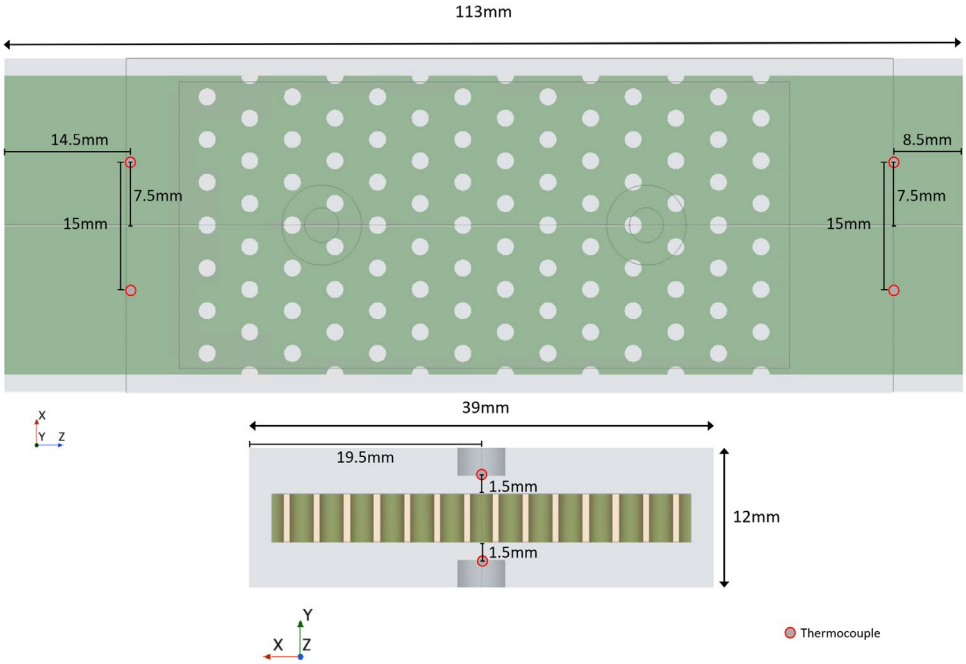

Figure 6: Thermocouple placement for the pin fin test section

Rig Loop Integration

After the electrical heating portions, the single jet impingement and pin fin array rigs were integrated at the hottest part of the loop. Here, the target inlet conditions are 200 bar and 400 Celsius. All tests follow a similar procedure. Before any CO_2 was introduced into the system, the system was placed under a vacuum to ensure no air or other impurities filled the system. After a vacuum state was held for a few minutes, CO_2 was introduced into the system from a CO_2 supply held within helium-padded tanks pressurized up to 2000 psi. After introducing the system with CO_2, the loop was pressurized using two single-action pumps in series to achieve the desired pressure. As the system was pressurizing, the loop's driving pump was engaged to begin the flow of CO_2. As the pressure continued to increase, all electrical heating was turned on to achieve the target pressure and temperature together. The loop could not be pressurized and then heated, as heating the gas increases the pressure, so achieving both simultaneously allowed the loop to reach operating conditions in a controlled manner. Testing could begin once operating conditions were achieved and all closed-loop components operated under stable conditions.

For impingement, this involved recording steady-state conditions of the test rig before engaging the mica heater to apply a constant heat flux into the system. The jet temperature was then calculated, and the surface temperature was extracted. This temperature difference allowed the heat transfer coefficient to be calculated and rig heat transfer measured. A similar process was adapted for the pin fin loop, but the methodology was to calculate the heat transfer of the test section. In the pin fin rig, an enthalpy balance approach was necessary. This was done by measuring the heat transfer across the pin fin array by recording the inlet and outlet temperatures upstream and downstream of the test section. The end wall temperature was also recorded using a strategically placed thermocouple at the center of the end wall. The wetted surface temperature was extrapolated from the thermocouple location using a simplified 1D Fourier's law of heat conduction approach. The wetted surface temperature and the bulk average temperature were used as the delta T in calculating the heat transfer coefficient for this rig. The details of both methodologies will be shown in the Results and Discussion sections.

RESULTS AND DISCUSSION

Before any sCO_2 cases were run, both test rig assemblies were validated using air to compare to existing literature correlations. This gave confidence in the rig design and was then instrumented into the sCO_2 loop for testing. Each experiment was designed to use the Nusselt number to quantify the heat transfer for the sCO_2 rig. However, both rigs required different approaches to reach this result.

Data Reduction

For heat transfer in the sCO2 environment, the heat transfer coefficient was necessary to calculate the Nusselt number. This was the case for both test rigs. Nusselt number is calculated with the heat transfer coefficient (h), the characteristic length was diameter for both test rigs (D), and the thermal conductivity of the fluid (k).

$$Nu = \frac{hD}{k} \quad (1)$$

The diameter for each case was defined as the jet orifice diameter for the impingement rig and

the pin diameter for the pin fin rig. The thermal conductivity was calculated based on the test case's temperature and pressure. These points were used in CoolProp [18], an open-source thermophysical property calculator that utilizes the same equations of state as other databases, such as RefPROP. This software can calculate the thermophysical properties of various fluids, which is essential for adequately representing the real gas nature of CO_2.

The heat transfer coefficient was necessary to calculate the Nusselt number, and acquiring this used two different methodologies for the respective test rigs. The heat transfer coefficient is calculated by taking the heat flux of the system and dividing that by the temperature difference between the wetted surface and bulk fluid temperature. This equation can be written as:

$$q'' = h(T_{wall} - T_{bulk}) \quad (2)$$

A different methodology was used to accommodate the testing configurations of each rig and calculate the heat transfer parameters. The wall temperature was extracted for the impingement rig using the linear approximation of temperature across the copper cylinder from the varying thermocouple locations. The bulk fluid temperature was extracted by accounting for heat loss in the plenum by observing the temperature difference across the plenum before and after a heat flux was applied. The heat flux of the system was calculated by taking the surface area of the impinging plate, and the power into the system was calculated from the applied voltage to the mica heater and measured resistance across the heater. This methodology can be seen in the following equations.

$$A_s = \pi r_s^2 \quad (3)$$

$$Q_s = \frac{V^2}{R} \quad (4)$$

$$Q_l = mdT + b \quad (5)$$

$$h = \frac{Q_s - Q_l}{A_s(T_{surface} - T_{jet})} \quad (6)$$

The heat loss (Q_l) was quantified in a separate study for the impingement plate configuration by varying the measured delta T across the copper block and ambient temperature. This resulted in a linear equation representing the assembly's heat loss for a given temperature difference. With the calculated heat transfer coefficient and the diameter of the jet, the Nusselt number could now be calculated for the single jet impingement rig.

An enthalpy balance approach was used for the pin fin array to reach the heat transfer coefficient. This was decided on since the instrumentation was limited to the upstream and downstream locations. This meant that assumptions needed to be made to capture the array heat transfer. The upstream and downstream temperatures needed to be recorded, and the resultant enthalpies (H) could be calculated using CoolProp, just as thermal conductivity could be. The enthalpy difference was used to calculate the heat flux of the system. The temperature difference of the heat transfer coefficient equation comes from the upstream and downstream temperatures, averaged to get a bulk temperature, as well as the end wall temperature, which was extrapolated from the measured location. This methodology did not need heat loss calculations, as it was observed that in this configuration, the system served as a heat sink, so instead of having a heat flux into the system, it could be assumed that all the heat flux was out of the system, flowing from the hot gas path into the ambient pressure vessel conditions. This

set of equations can be seen below.

$$q" = \frac{Q}{A_{wetted}} = \frac{\dot{m}}{A_{wetted}}(H_{upstream} - H_{downstream}) \quad (7)$$

$$T_{bulk} = \frac{T_{upstream} - T_{downstream}}{2} \quad (8)$$

$$T_{wall} = q"(\frac{l}{k_{SS}}) + T_{measured} \quad (9)$$

$$k_{SS} = (8.116E\text{-}2 + 1.618E\text{-}4\, T_{measured}) * 100 \quad (10)$$

Since the measured wall temperature was 1.5mm from the wetted surface, the temperature at the surface had to be extracted. The thermal conductivity of the stainless-steel end wall could be calculated from the measured wall temperature using an equation developed by Choong S Kim [19]. He developed several equations that allowed for the thermophysical properties of stainless steel to be calculated based on the temperature of the material. This allowed for a more accurate estimation of temperature of thermal conductivity for Fourier's law of thermal conduction.

Nusselt number is traditionally a function of the Reynolds number when looking at a complete rig heat transfer. Reynolds number was derived from the mass flow rate of each independent case. The velocity could be calculated from the mass flow rate. The equation for the Reynolds number is:

$$Re_D = \frac{\bar{\rho}\bar{u}_{max}D}{\bar{\mu}} \quad (11)$$

The density ($\bar{\rho}$) and dynamic viscosity ($\bar{\mu}$) were both properties that could be calculated using CoolProp, and the velocity was calculated from the mass flow rate. The diameter (D) is the respective characteristic length for each test rig.

Uncertainty for all experimental testing for both rigs was calculated using the methodology defined by the standards of Uncertainty Standard PTC 19.1-2013 by the American Society of Mechanical Engineers (ASME) [20]. The uncertainty can be generalized as:

$$u_\alpha = \sqrt{\sum_{i=1}^{n}(\theta_i u_i)^2} \quad (12)$$

Here, the α is the target variable for the uncertainty analysis. The Reynolds and Nusselt numbers were the two targets for calculating uncertainty in these experimental investigations. θ is the sensitivity of the i^{th} dependent variable that impacted the total uncertainty for the target. Uncertainty for each rig will be discussed in their respective sections.

Single Jet Impingement Heat Transfer

Single jet impingement sCO_2 heat transfer comprised ten cases that met the targeted criteria of a 400 C inlet temperature and 200 bar inlet pressure. Not all cases met the criteria but were plotted to serve as references for trend continuation at much higher Reynolds numbers and to fill in gaps. These cases can be seen in Table 3, where the green cases met the testing criteria, and the yellow cases deviated from the criteria. However, they were still plotted, and the orange cases were plotted for reference only due to high uncertainty. One of the yellow cases was at half pressure with the criteria inlet temperature, but the results did not deviate from the

observed trends. This was because the pressure deviation was much smaller for each isobar at the temperature range that the tests were conducted. This can also be attributed to the linear behavior of the thermophysical properties with significantly smaller slopes than when compared to the thermophysical property behavior near the critical point. This can be seen in Figure 7, where the thermophysical properties of density, thermal conductivity, specific heat, and dynamic viscosity were plotted.

Reynolds Number	Inlet Conditions P (bar), T (°C)	Temperature Delta (°C)	Nusselt Uncertainty (%)
82,932	117, 154	53.5	4
256,147	203, 204	15	10
197,393	95, 412	10.6	21
249,984	209, 416	7.7	29
401,103	197, 415	5.2	44
470,112	179, 413	4.9	43
583,443	191, 405	4.2	50
601,530	202, 400	4.0	51
638,993	203, 320	3.2	64
1,157,380	197, 225	2.6	62

Table 3: Experimental cases for single jet impingement.

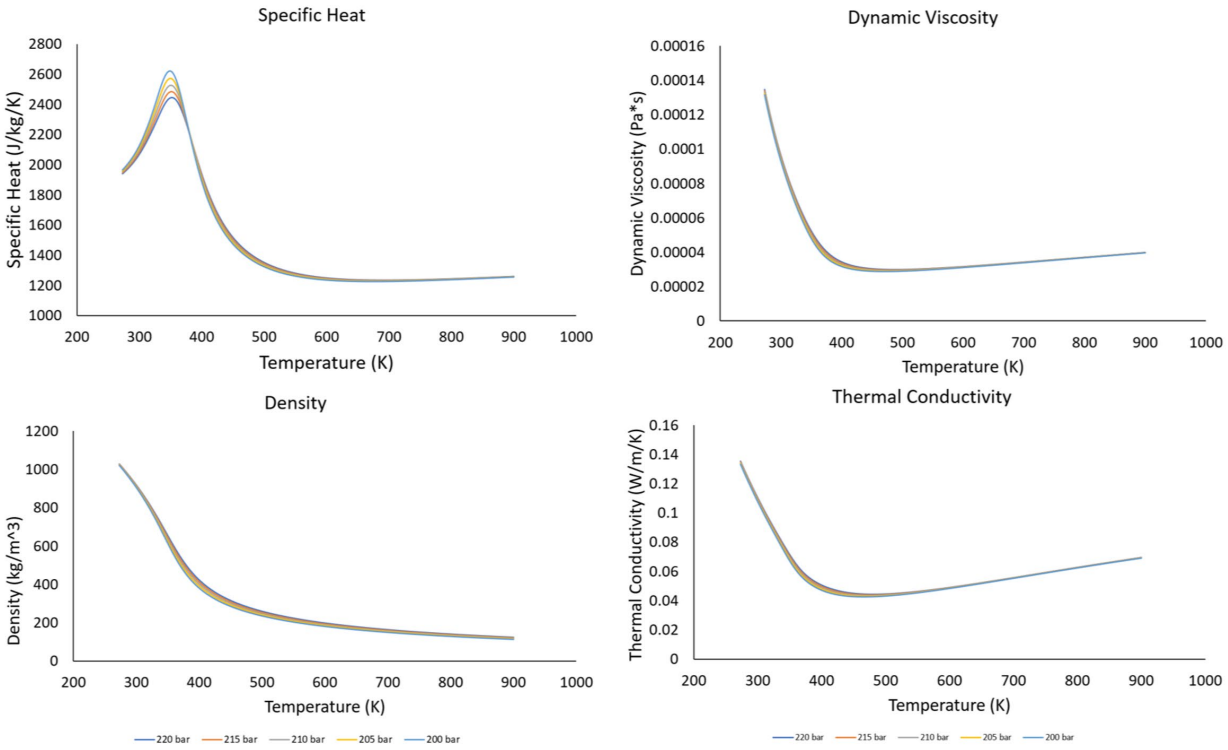

Figure 7: Thermophysical properties for sCO_2 from before the critical point to beyond the test regime of 400 Celsius (673 Kelvin)

The sCO_2 test cases were all run at a z/D of 2.8. The resultant Nusselt number was plotted against the correlations derived using air data in literature. This can be seen in Figure 8, where all cases were plotted and compared to the correlations derived from air data in literature. As the Reynolds number increased, the heat transfer deviation between the air correlations and sCO2 experimental data continued to increase. This deviation was tabulated in Table 3, where the Nusselt number increased deviation between sCO2 and air can be observed. Uncertainty was also tabulated for each case and can be seen in Table 3.

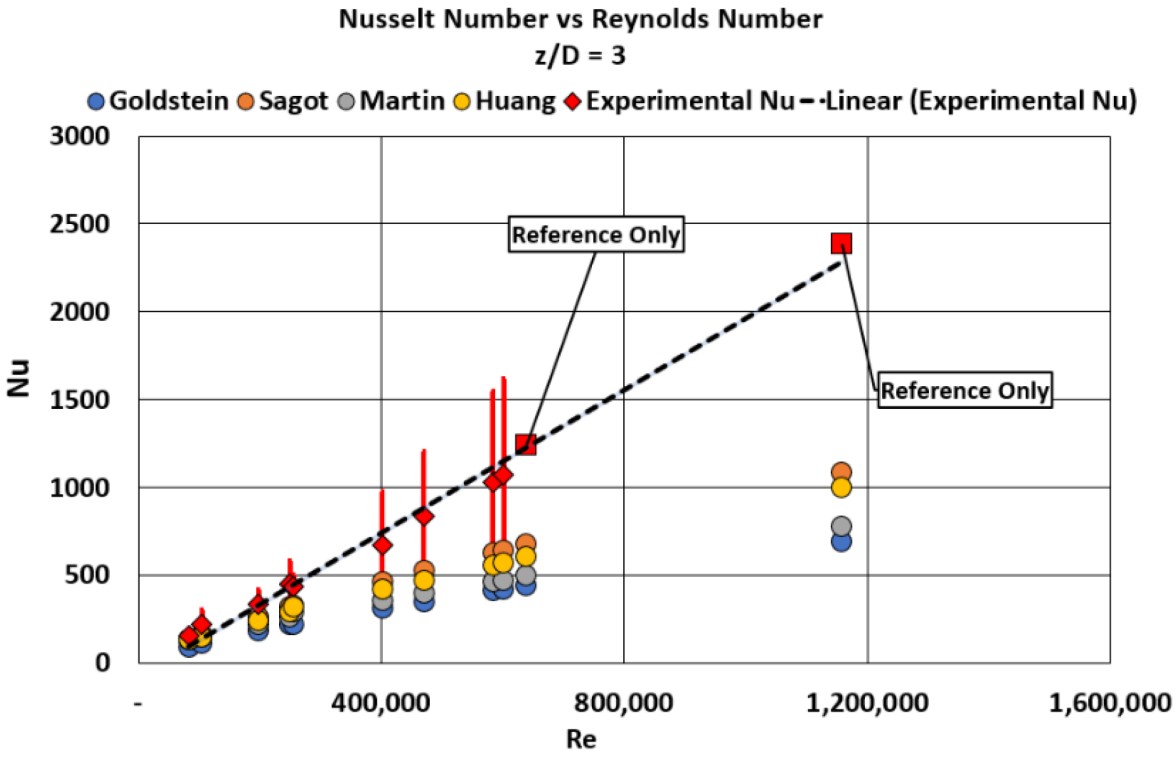

Figure 8: Experimental data for sCO_2 compared to correlations derived from air data in literature

The experimental data was also compared to CFD models to validate sCO_2 methodology for building numerical modeling of the real gas sCO_2 behavior. Two software were looked at, these being StarCCM+ and Ansys FLUENT. A $1/8^{th}$ model was constructed to represent the gas path and compare the heat transfer seen at matching Reynolds numbers to the experimental results. The experimental results defined the boundary conditions for each model to allow for a direct comparison. It was found that both StarCCM+ and Ansys FLUENT agreed well with the experimental results, giving confidence in the modeling capabilities of capturing sCO_2 as a real gas in this supercritical regime. The overlayed CFD model results can be seen plotted over the experimental results in Figure 9.

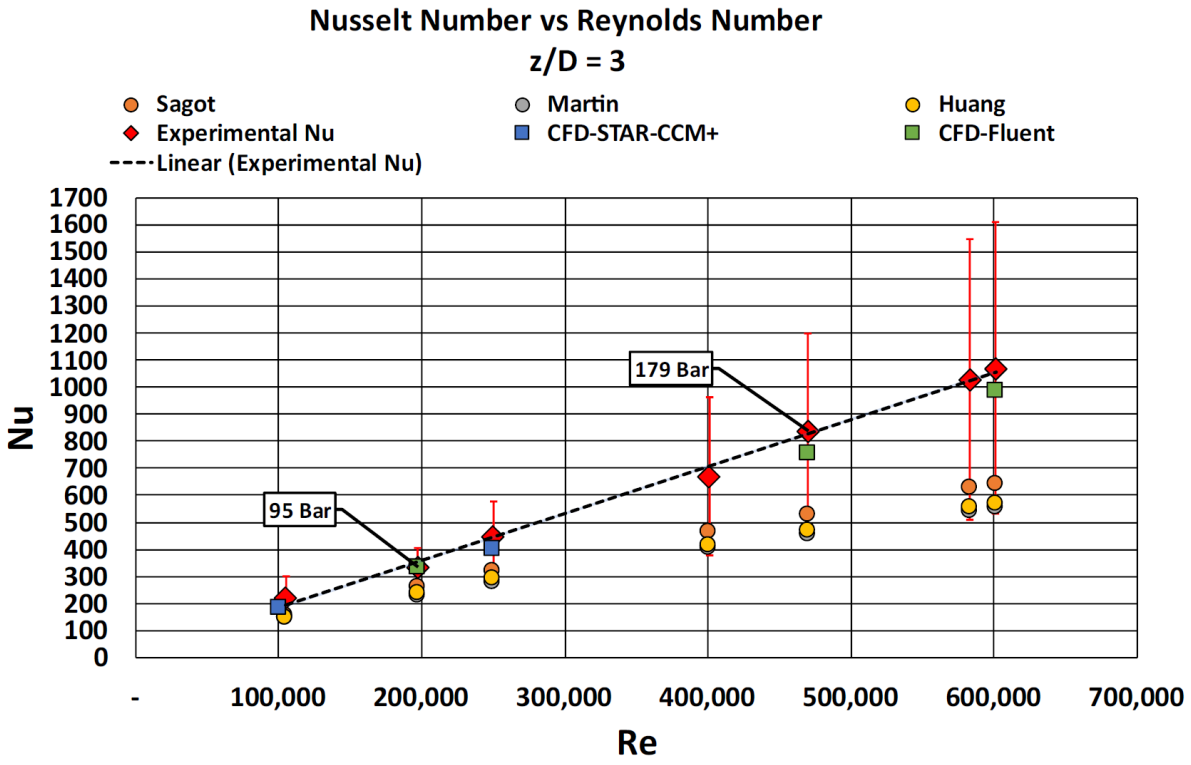

Figure 9: Experimental and numerical data points showing a tight agreeance between experimental and numerical results

Considering that the existing heat transfer correlations for single jet impingement could not capture the heat transfer effects in the sCO_2 working environment, a modified correlation was constructed to fit the experimental results better. This correlation was adopted from the Martin correlation and could be stated as:

$$Nu_{avg} = Pr^{0.42}\frac{D}{r}\frac{1-1.1\frac{D}{r}}{1+0.1(\frac{H}{D}-6)\frac{D}{r}}0.151Re^{n} \quad (13)$$

$$for\ 100{,}000 < Re < 360{,}000, use\ n = 0.8158$$

$$for\ 360{,}000 < Re < 601{,}000, use\ n = 0.8253$$

$$T_{jet} \approx 400\ C, 95 < P_{bar} < 210, \frac{H}{D} \approx 2.8$$

This adjusted correlation was plotted with the experimental data to see how the adjusted correlation fit with the experimental data. This can be seen in Figure 10.

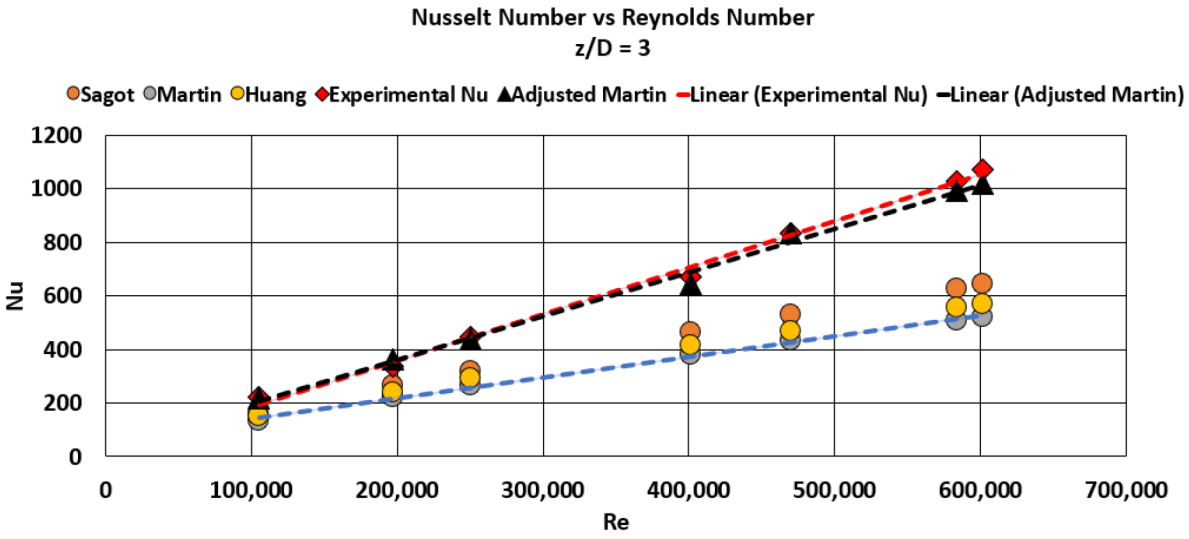

Figure 10: Experimental data plotted with the adjusted Martin correlation to better fit the sCO_2 data set

Since correlations derived from air data could not represent the heat transfer for single jet impingement, investigating other internal cooling geometry was warranted to see if these observations carried over to other geometric features. This led to the development and testing of the pin fin rig.

Staggered Pin Fin Heat Transfer

The pin fin array presented several challenges when designing the experimental methodology for capturing the heat transfer across this rig. The pin fin testing matrix consisted of three achievable cases targeting a Reynolds number spread of approximately 25,000 to 66,000. This test matrix can be seen in Table 4.

Reynolds Number	Inlet Conditions P (bar), T (°C)	Nusselt Uncertainty (%)
25,096	201, 406	68
49,910	206, 406	67
66,602	208, 401	89

Table 4: Experimental test matrix for staggered pin fin array

Plotting the resultant heat transfer with the respective Reynolds number in conjunction with the experimental correlation derived by Metzger for a similar geometry in an air environment. It was also plotted with the trend line for a local row averaged Nusselt number approach

performed on a matching geometric pin fin array in a conjugate heat transfer numerical investigation performed by Wardel et al. [17]. This can be seen in Figure 11.

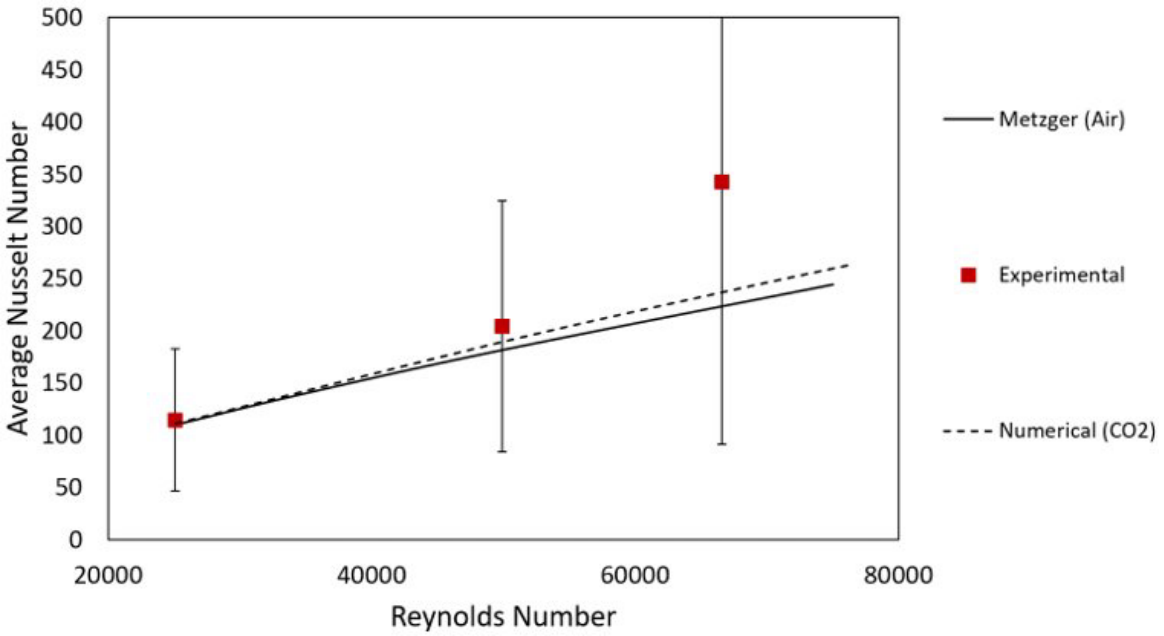

Figure 11: Experimental results plotted alongside Metzger correlation derived from air data in literature and numerical investigations performed by Wardel et al [?]

One of the critical challenges in this test rig configuration was achieving a temperature difference significant enough to minimize uncertainty. Unfortunately, this was not achievable with the limited instrumentation and limited power input from the mica heaters; this is why a heat sink approach was used with all heat flux assumed to be out of the system. Despite efforts to create a significant temperature difference, large uncertainty values were unavoidable in this test configuration. These uncertainty values can be seen in Table 4. A conjugate numerical approach was necessary to explore the heat transfer behavior between sCO_2 and air in the pin fin array further. Since the sCO_2 modeling techniques were explored and validated with the impingement rig, confidence in the numerical methodology for capturing the real gas effects of sCO_2 was achieved despite this being a different geometry. This does not replace the need to validate the numerical space with this geometry once more robust experimental results are available. However, it allowed for a preliminary investigation into the pin fin heat transfer for the sCO_2 working environment. The numerical model was designed with matching geometry, and the boundary conditions of the conjugate problem were directly derived from the experimental setup so that side-by-side comparisons between experimental and numerical results could be compared. The first observation when going to the numerical setup was the effects of extracting the temperature of the wetted end wall surface when compared to using the measure wall temperature. The idea behind this was to observe how, by extrapolating the temperature to the wetted surface, the results represented a Nusselt number closer to experimental results and past numerical investigations, at least for cases below 50,000. Beyond this point, the uncertainty continued to climb, reducing the capability to fully capture these effects experimentally. This observation can be found in Figure 12.

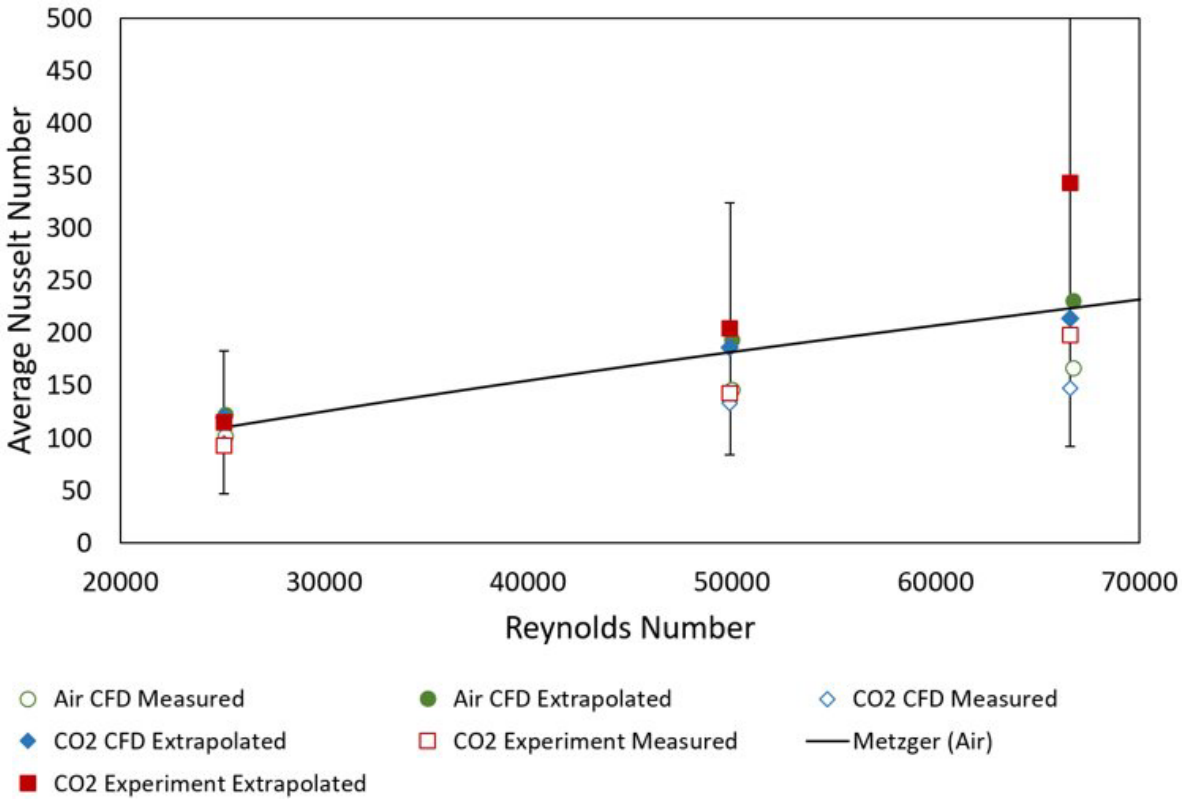

Figure 12: Experimental and Numerical comparison for air and sCO_2

Initial numerical findings found by Wardell et al. [17] suggested a deviation such as was observed in the single jet impingement results between air and sCO_2; however, this deviation was much smaller comparably. It was also observed that these deviations were washed out in this whole array approach to calculating the Nusselt number using an enthalpy balance and a total array heat flux. Air and sCO_2 performed very similarly to one another at matching Reynolds numbers. This was shown in Figure 13, where the heat flux definition was changed from the full exterior array, including the upstream and downstream channels, to being localized to just above the pin fin boundaries by localizing the heat flux, which closely resembled the methodology in literature for pin fin experimentation in the air regime, a slight deviation returned between sCO_2 and air.

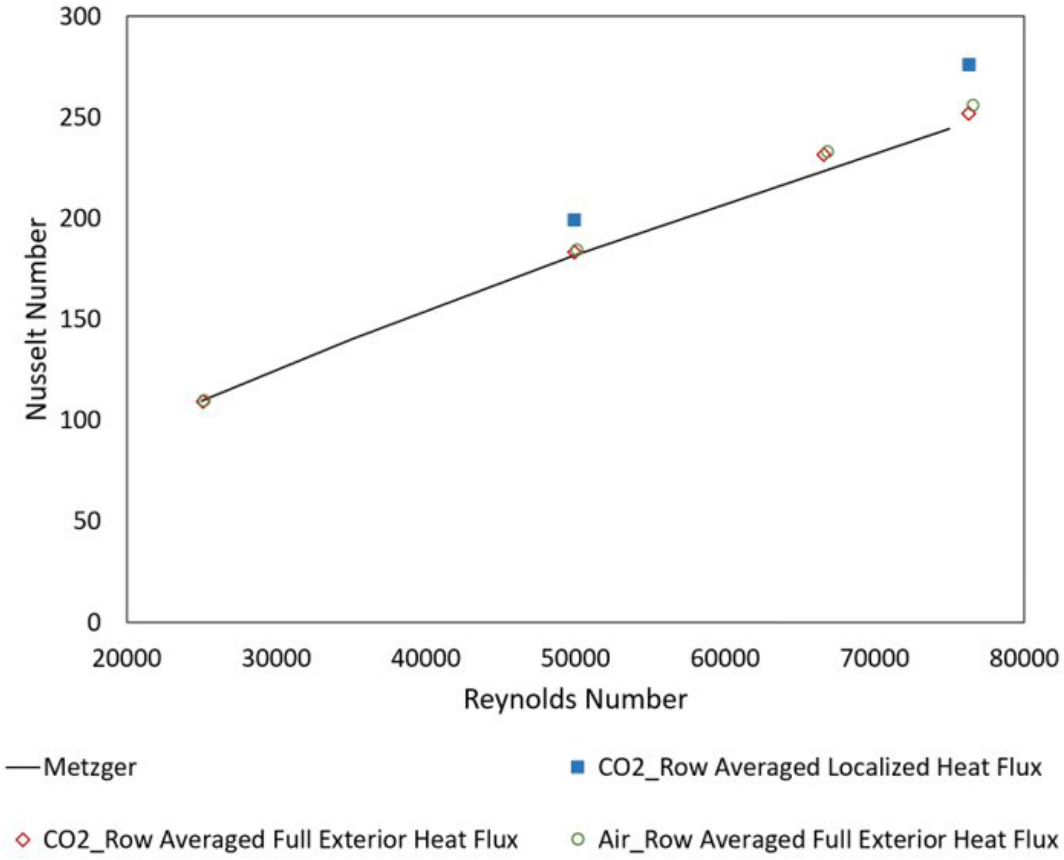

Figure 13: Comparing Nusselt number between local and full exterior heat flux

To further explore this observation, isolating the differences between sCO_2 and air local to the pin fin rows was necessary. The first step to doing this was comparing the Nusselt number between the localized heat flux located just above the pin fin domain to the full array feat flux definition that represented all exterior walls from the upstream and downstream thermocouple locations, which represented the experimental approach of allowing heat to flow out of the test section. By comparing these two heat flux definitions, it was observed that when the heat flux was isolated to the pins, the first four to five rows showed higher heat transfer than when compared to the total exterior heat flux definition. This indicated that the end walls upstream and downstream had a diluting effect on the array heat transfer compared to the localized heat flux definition, as seen in Figure 14. This would warrant further investigation into the fundamental development in the sCO_2 working environment.

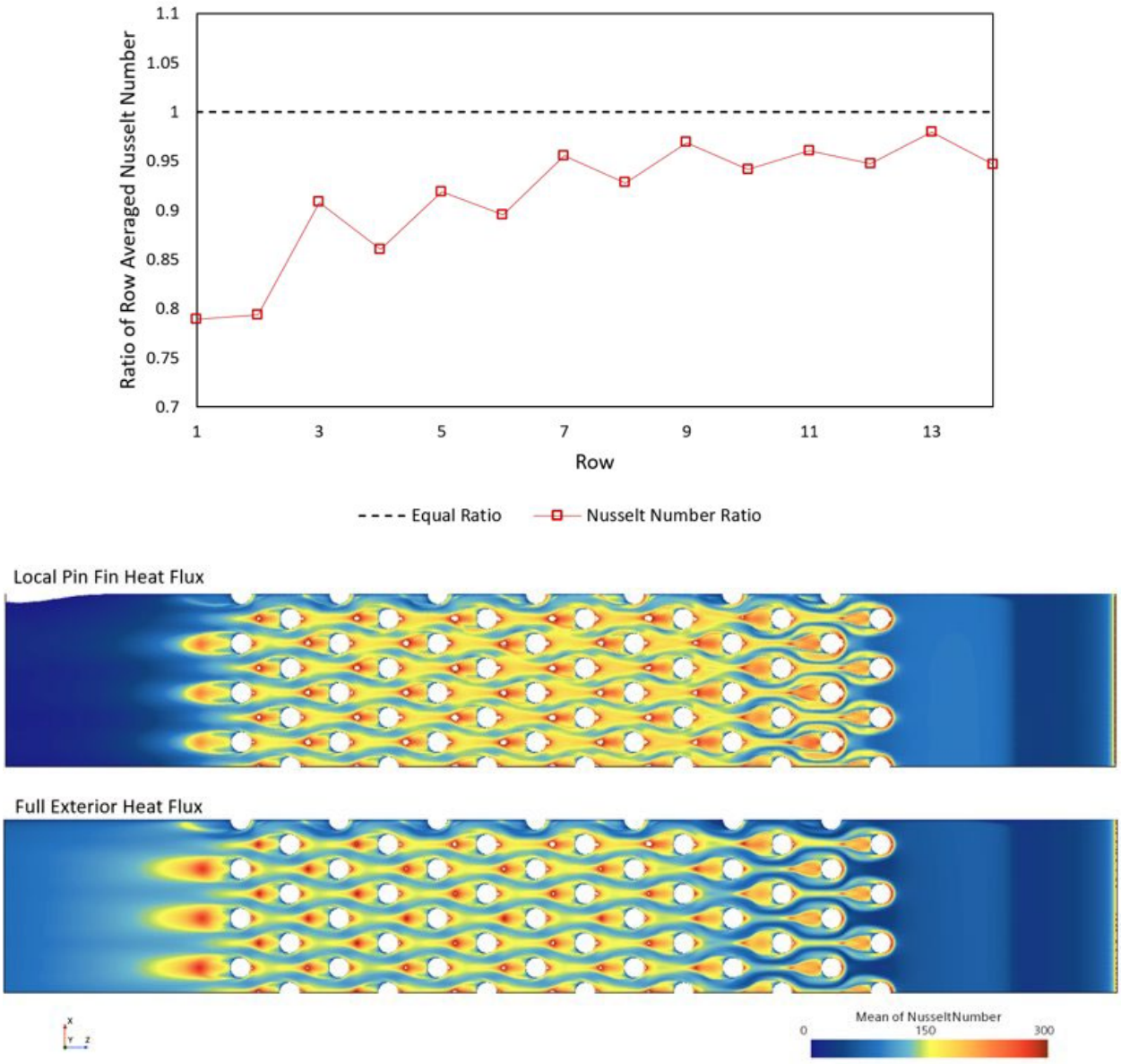

Figure 14: Contour comparison of heat transfer development comparing local and full exterior heat flux locations

Unlike in single jet impingement, where a considerable increase in heat transfer was observed in the sCO2 environment, the deviations between air and sCO2 are much more minor in the pin fin array. This could be attributed to several factors that need further investigation.

CONCLUSIONS

Supercritical carbon dioxide presents several advantages to gas turbine cycle technology. Operating temperatures need to rise to continue increasing the thermal efficiency of these cycles. This introduces the need to include internal cooling features in the sCO2 turbine design. These features need to be investigated again in the new working environment, as this real gas

behavior cannot be assumed to be represented by correlations derived from air data.

Revisiting heat transfer behavior in single jet impingement and pin fin array for internal cooling in the sCO2 working environment verifies that the correlations derived from air data in literature cannot be assumed to represent these features for heat transfer behavior. The first geometry, single jet impingement, significantly deviated from the existing correlations for this feature. It showed that as Reynolds's number increased, the difference between air and sCO2 grew, trending at a steeper slope than air. This led to modifying the Martin correlation to capture the sCO2 heat transfer better. In the computational space, it was observed that modeling the real gas behavior of sCO-2 was able to capture the heat transfer behavior in both StarCCM+ and Ansys FLUENT reliably.

Seeing the enhanced heat transfer for single jet impingement served as motivation to explore other geometric features further. For the pin fin array, the experimental setup had several challenges that limited the ability to capture the local effects of heat transfer through the pin fin array, as is traditionally done in literature for these features. A control volume approach using enthalpy balance captured a bulk behavior, but the uncertainty for these experimental cases was much higher than desired. In the pin fin array, it was observed that the sCO2 and air heat transfer had a much smaller difference between the two working mediums. In the computation space, a more local investigation could be performed. When processing these models using the experimental methodology, similar results were seen at a Reynolds number of 50000 and below for both CFD and experimental. When processed locally, the differences between sCO2 and air presented themselves, but to experimentally explore this, further investigations would be needed using a simplified rig and more instrumentation to capture local effects.

Overall, the internal cooling features must be re-investigated in the sCO2 working environment, as the differences between sCO2 and air cannot be predicted for each geometric feature. Single jet impingement shows an increased deviation in heat transfer between the two working mediums; however, for pin fin arrays, this deviation is much smaller and washed out in a control volume approach.

ACKNOWLEDGEMENTS

This material is based upon work supported by the Department of Energy, United States of America, under award number DE-FE0031929. This paper was prepared as a part of work sponsored by an agency of the United States Government in partnership with Southwest Research Institute, General Electric Global Research Center, 8Rivers Capital LLC, Air Liquide, the Electric Power Research Institute, the University of Central Florida, and Purdue University. M. Otto would like to acknowledge further the support from the University of Central Florida's Preeminent Postdoctoral Program (P3). Lastly, the authors acknowledge the University of Central Florida Advanced Research Computing Center for providing computational resources and support that contributed to the results reported herein. URL: https://arcc.ist.ucf.edu

DISCLAIMER

trademark, manufacturer, or otherwise does not necessarily constitute or imply its endorsement, recommendation, or favoring by the United States Government or any agency thereof. The views and opinions of authors expressed herein do not necessarily state or reflect those of the United States Government or any agency thereof.

REFERENCES

[1] White, Martin T., Giuseppe Bianchi, Lei Chai, Savvas A. Tassou, and Abdulnaser I. Sayma. 2021. "Review of supercritical CO2 technologies and systems for power generation." *Applied Thermal Engineering.*

[2] Crespi, Francesco, Giacomo Gavagnin, David Sanchez, and Gonzalo S. Martinez. 2017. "Supercritical carbon dioxide cycles for power generation: A review." *Applied Energy.*

[3] Net Power Inc. 2023. *La Porte Test Facility.* https://netpower.com/la-porte-test-facility/.

[4] Lariviere, B., Marion, J., Macadam, S., McDowell, M., Lesemann, M., McClung, A., and Mortzheim, J., 2021. “sco2 power cycle development and step demo pilot project”. 4th European sCO2 Conference for Energy Systems: March 23-24, 2021, Online Conference, Mar, p. 352–362

[5] Moore, Jeffrey, Josh Neveu, Jason Bensmiller, Cole Replogle, Jianliang Lin, Jeremy Fetvedt, Ian Cormier, Jayanta Kapat, Erik Fernandez, and Guillermo Paniagua. 2023. "DEVELOPMENT OF A 300 MWE UTILITY SCALE OXY-FUEL SCO2 TURBINE." *ASME Turbo Expo 2023.*

[6] Martin, H., 1977, “Heat and Mass Transfer between Impinging Gas Jets and Solid Surfaces,” Advances in Heat Transfer, Elsevier, pp. 1–60.

[7] Huang, L., and El-Genk, M. S., 1994, “Heat Transfer of an Impinging Jet on a Flat Surface,” Int. J. Heat Mass Transfer., 37(13), pp. 1915–1923.

[8] Sagot, B., Antonini, G., Christgen, A., and Buron, F., 2008, “Jet Impingement Heat Transfer on a Flat Plate at a Constant Wall Temperature,” Int. J. Therm. Sci., 47(12), pp. 1610–1619.

[9] Goldstein, R. J., Behbahani, A. I., and Heppelmann, K. K., 1986, “Streamwise Distribution of the Recovery Factor and the Local Heat Transfer Coefficient to an Impinging Circular Air Jet,” Int. J. Heat Mass Transf., 29(8), pp. 1227–1235.

[10] Chyu, M. K. 1989. "Heat Transfer and Pressure Drop for Short Pin-Fin Arrays with Pin-Endwall Fillet." *Gas Turbine and Aeroengine Congress and Exposition.*

[11] Ames, F. E., L. A. Dvorak, and M. J. Morrow. 2005. "Turbulent Augmentation of Internal Convection Over Pins in Staggered-Pin Fin Arrays." *Journal of Turbomachinery.*

[12] Metzger, D. E., and S. W. Haley. 1982. "Heat Transfer Experiments and Flow Visualization for Arrays of Short Pin Fins." *ASME Turbo Expo 1982.*

[13] Otto, Marcel. 2019. "IMPROVING TURBINE PERFORMANCE: A CONTRIBUTION TO THE UNDERSTANDING OF HEAT TRANSFER AND VORTICAL STRUCTURES IN

STAGGERED PIN FIN ARRAYS."

[14] VanFossen, G. J., 1982. “Heat-Transfer Coefficients for Staggered Arrays of Short Pin Fins”. Journal of Engineering for Power, 104(2), 04, pp. 268–274.

[15] Richardson, John, Ryan Wardell, Erik Fernandez, and Jayanta Kapat. 2023. "Experimental and Computational Heat Transfer Study of sCO2 Single-Jet Impingement." *ASME Turbo Expo 2023.*

[16] Wardell, R. J., Richardson, J., Otto, M., Smith, M., Fernandez, E., and Kapat, J. “An Experimental Investigation of Heat Transfer for Supercritical Carbon Dioxide Cooling in a Staggered Pin Fin Array”. *Proceedings of the ASME Turbo Expo 2023: Turbomachinery Technical Conference and Exposition. Volume 12: Supercritical CO2*. Boston, Massachusetts, USA. June 26-30, 2023. V012T28A022. ASME.

[17] Wardell, R. J., Otto, M., Smith, M., Fernandez, E., and Kapat, J., 2022. “A Numerical Study on Conjugate Heat Transfer of Supercritical Carbon Dioxide Cooling in a Staggered Pin Fin Structure”. Vol. Volume 6B: Heat Transfer — General Interest/Additive Manufacturing Impacts on Heat Transfer; Internal Air Systems; Internal Cooling of Turbo Expo: Power for Land, Sea, and Air. V06BT15A015.

[18] Bell, I. H., J. Wronski, S. Quoilin, and V. Lemort. 2014. "Pure and pseudo-pure fluid thermophysical property evaluation and the open-source thermophysical property library." *Industrial & Engineering Chemistry Research* 2498-2508.

[19] Kim, Choong S. 1975. "Thermophysical Properties of Stainless Steels ."

[20] ASME. 2014. "Test Uncertainty." New York, NY.